Multiple Magnetoionic Regimes in Ta/Co20Fe60B20/HfO2

Multiple Magnetoionic Regimes in $Ta/Co_{20}Fe_{60}B_{20}/HfO_2$

R. Pachat,[1] D. Ourdani,[2] J.W. van der Jagt,[3] M.-A. Syskaki,[4] A. Di Pietro,[5] Y. Roussigné,[2] S. Ono,[6] M.S. Gabor,[7] M. Chérif,[2] G. Durin,[5] J. Langer,[4] M. Belmeguenai,[2] D. Ravelosona,[1,3] and L. Herrera Diez[1,*]

[1] *Centre de Nanosciences et de Nanotechnologies, CNRS, Université Paris-Saclay, 91120 Palaiseau, France*
[2] *Laboratoire des Sciences des Procédés et des Matériaux, CNRS-UPR 3407, Université Paris 13, Sorbonne Paris Cité, 93430 Villetaneuse, France*
[3] *Spin-Ion Technologies, C2N, 10 Boulevard Thomas Gobert, 91120 Palaiseau, France*
[4] *Singulus Technologies AG, Hanauer Landstrasse 103, 63796, Kahl am Main, Germany*
[5] *Istituto Nazionale di Ricerca Metrologica, Strada delle Cacce 91 10135, Torino, Italy*
[6] *Central Research Institute of Electric Power Industry, Yokosuka, Kanagawa 240-0196, Japan*
[7] *Center for Superconductivity, Spintronics and Surface Science, Physics and Chemistry Department, Technical University of Cluj-Napoca, Cluj-Napoca RO-400114, Romania*

(Received 29 January 2021; revised 2 April 2021; accepted 2 June 2021; published 22 June 2021)

In $Ta/(Co,Fe)B/HfO_2$ stacks, a gate voltage drives, in a nonvolatile way, the system from an underoxidized state exhibiting in-plane anisotropy (IPA) to an optimum oxidation level resulting in perpendicular anisotropy (PMA) and further into an overoxidized state with IPA. The IPA $\rightarrow$ PMA regime is found to be significantly faster than the PMA $\rightarrow$ IPA regime, whereas only the latter shows full reversibility under the same gate voltages. The effective damping parameter also shows a marked dependence with gate voltage in the IPA $\rightarrow$ PMA regime, going from 0.029 to 0.012, and only a modest increase to 0.014 in the PMA $\rightarrow$ IPA regime. The existence of two magnetoionic regimes has been linked to a difference in the chemical environment of the anchoring points of oxygen species added to underoxidized or overoxidized layers. Our results show that multiple magnetoionic regimes can exist in a single device and that their characterization is of great importance for the design of high-performance spintronics devices.

DOI: 10.1103/PhysRevApplied.15.064055

I. INTRODUCTION

Controlling magnetic properties with electric (E) fields is of great importance for spintronics applications due to its potential for lowering power consumption in memory prototypes. It has been shown that E-field-induced charge accumulation can lead to important changes in magnetic anisotropy [1–4], which can be used to reliably control domain wall (DW) pinning and velocities [5,6], and assist the magnetization switching in magnetic tunnel junctions [7] in ferromagnetic (FM) metallic films. More complex mechanisms such as switching between FM and skyrmionic states [8,9] have also been demonstrated, where the E-field control of the Dzyaloshinskii-Moriya interaction (DMI) [10,11] is also at play.

In addition to the effects of charge accumulation, magnetoionics can also provide nonvolatility and a more extended effect over the entire magnetic layer, unlike charge accumulation, limited by electrostatic screening [12]. Large magnetoionic effects in magnetic anisotropy can be achieved, including a spin reorientation transition, which applied to DW motion can be used to create nonvolatile and very efficient DW traps [13,14]. In addition, magnetoionic control of spin accumulation [15] and DMI [16] has been demonstrated as well as DW chirality switching in a controlled oxygen atmosphere [17], which is of capital importance for implementing E-field-assisted spin-orbit torques in devices. In these ionic materials, the migration of oxygen [14,18] or hydrogen species [19] is at the heart of the ionic effects observed, which have recently been shown to offer operation speeds close to 1 ms [20].

The interest in nonvolatility for spintronics applications goes hand in hand with magnetoionic reversibility. Recently, studies have focused on the magnetoionic reversibility variations between oxides [21], pointing out the importance of the differences in the mechanisms governing ionic conduction. A deep understanding of the mechanisms of reversibility in magnetoionics is therefore needed to design high-performance magnetoelectric devices. In this study, we unveil a higher degree of complexity in HfO_2-based devices, where two distinct magnetoionic regimes have been identified in a single structure.

*liza.herrera-diez@c2n.upsaclay.fr

In addition, we also shine light on the magnetoionic effects on the effective damping parameter α_{eff}, largely overlooked in the literature and of great importance for fast magnetization dynamics. We show that α_{eff} can be reduced significantly by inducing ionic motion and that its lowest value (0.012) coincides with the appearance of PMA.

The magnetic materials used in this study are amorphous Ta(5 nm)/$Co_{20}Fe_{60}B_{20}$(1 nm)/HfO_2(3 nm) films grown by magnetron sputtering, all samples investigated here were cut from the same wafer. The ionic liquid (IL) [EMI][TFSI] (1-ethyl-3-methylimidazolium bis(trifluoromethanesulfonyl)imide) is added to the surface of the film to incorporate the IL gate, which can provide high E fields that have been shown to induce ionic motion in a variety of materials [22–24]. The thickness of the IL is macroscopic, in the range of several hundreds of micrometers. However, the effective IL thickness is estimated taking into account only the distance over which an electric double layer is formed at the side of each of the electrodes, which is 1 nm [25]. A counter electrode, a glass substrate coated with a 100-nm-thick indium tin oxide (ITO) layer is subsequently placed on top of the IL. The size of the E-field biased area is about 0.25 cm^2. Samples were stored in air and at room temperature before conducting the gating experiments if not indicated otherwise. The hysteresis loops have been measured by anomalous Hall effect using a bias current of 400 μA. All magnetic states presented here are nonvolatile, all measurements were conducted after switching off the gate voltage. A graphic representation of the device geometry is presented in Fig. 1.

In the initial state, before exposure to the gate voltage, the magnetic layers are underoxidized, exhibiting in-plane magnetic anisotropy (IPA). Under the action of a negative gate voltage applied to the top ITO electrode a first regime (I) is identified, in which IPA transitions into PMA, followed by a second regime (II) where further oxidation

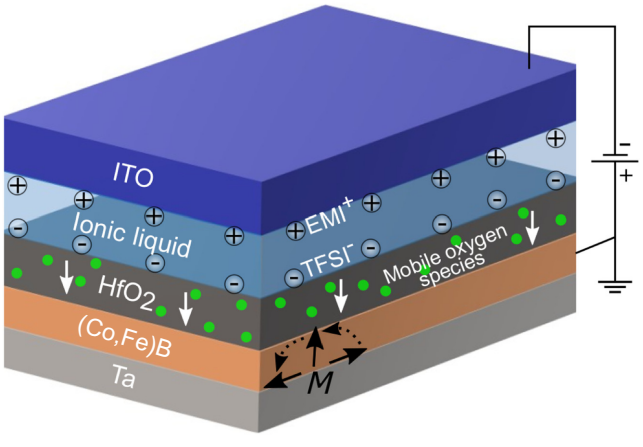

FIG. 1. Graphic representation of the magnetoionic stack covered with the ionic liquid $[EMI]^+[TFSI]^-$ gate. The gate voltage induces the motion of oxygen species in HfO_2.

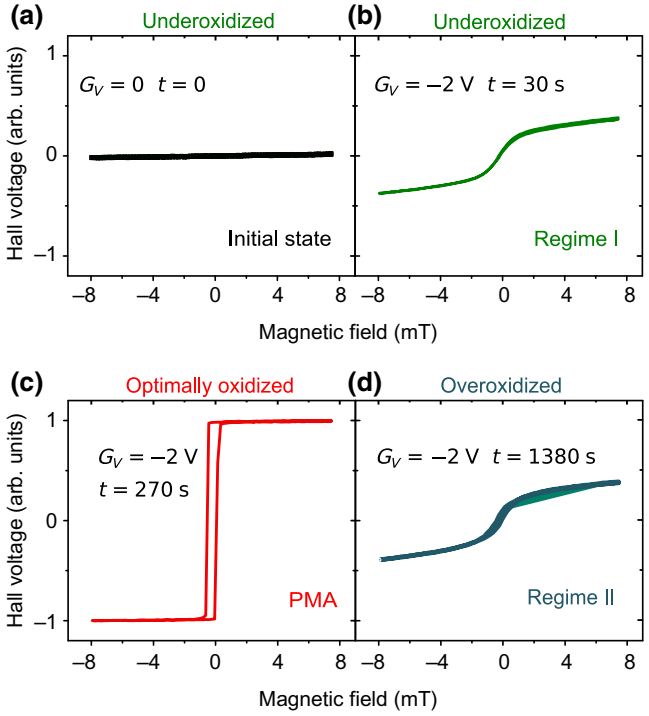

FIG. 2. A progressive oxidation is induced upon exposure to a gate voltage $G_V = -2$ V. Different exposure times t drive the system from IPA (a, initial state) through regime I (b) into PMA (c) and back to IPA through regime II (d).

drives PMA into IPA. This entire anisotropy evolution is presented in Fig. 2 with the corresponding cumulative biasing times for each case, these values correspond to the accumulated time of all previous operations. The gate voltage $G_V = -2$ V was applied for a total accumulated time of $t = 1380$ s. It is well known that thin magnetic films can exhibit a window of oxidation levels at the interface with an oxide which promotes PMA, whereas underoxidation or overoxidation will result in IPA [26]. Oxygen species are also known to migrate from the HfO_2 toward the (Co, Fe)B layer under gate voltages, as reported for other HfO_2-based devices [16,27], therefore oxygen migration is thought to be at the heart of the effects observed here. In the following, we describe in detail the two magnetoionic regimes and the effect of ionic diffusion on the effective damping parameter α_{eff}.

II. MAGNETOIONIC REGIMES I AND II

Figure 3(a) shows the time dependence of the out-of-plane remanence percentage, where 100% corresponds to the Hall voltage at zero applied magnetic field in the PMA state, for the entire anisotropy range going from the initial underoxidized IPA state through regime I (positive slope), PMA (the point of highest remanence), and regime II (negative slope) to finish in an overoxidized IPA state.

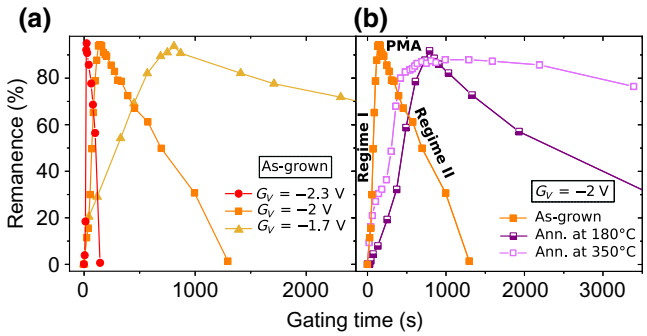

FIG. 3. Remanence as a function of gating time in (a) as-grown samples under $G_V = -2.3$ V (circles), $G_V = -2$ V (squares), and $G_V = -1.7$ V (triangles). (b) Samples annealed at 180 °C (half open squares) and 350 °C (open squares) under $G_V = -2$ V.

As-grown samples have been investigated under three different constant gate voltages of $G_V = -2.3$ V (circles), $G_V = -2$ V (squares), and $G_V = -1.7$ V (triangles). The speed of the entire process critically increases for higher gate voltages, responding to a stronger driving force for ionic motion. For all applied gate voltages, the magnetoionic process in regime I is significantly faster than in regime II. This difference in the time evolution as a function of gate voltage between regime I and II could be linked to a difference in the chemical environment, and thus of anchoring, of the oxygen species interacting with the (Co, Fe)B layer in regimes I and II. In regime I, the energy barrier associated with adding oxygen species to the underoxidized (Co, Fe)B interface may be lower than in regime II, where oxygen species have to be added to an already optimally oxidized (Co, Fe)B interface.

Measurements were also conducted using underoxidized samples that were annealed before applying a gate voltage of −2 V, these measurements are presented in Fig. 3(b). An underoxidized sample was annealed at 180 °C (open squares) for 1 hour to reduce moisture without inducing the crystallization of the (Co, Fe)B. Under $G_V = -2$ V, the speed of the ionic process in both regimes I and II was critically reduced, while still showing the same difference discussed previously between regimes I and II. This has been linked to a contribution to the mobile oxygen species coming from air humidity, a feature observed in ionic systems based on hydrogen mobility [19]. A sample annealed at 350 °C (half open squares) for 1 hour was also investigated under $G_V = -2$ V. These annealing conditions are known to induce the formation of crystallized grains in (Co, Fe)B/MgO stacks, where the MgO layer acts as a crystallization template [28,29], and the migration of B towards the Ta substrate [30]. In (Co, Fe)B/HfO_2, a similar behavior could be tentatively proposed, where B diffusion [31] and the formation of crystalline grains would have an effect on ionic mobility. Figure 3 shows that annealing has an effect on ionic dynamics in this system, regime I is slower than in the as-grown sample whereas regime II is significantly slower with respect to all other samples investigated. As mentioned earlier, the chemical environment of the mobile oxygen species at their anchoring points in the (Co, Fe)B layer is likely to be nonequivalent in regimes I and II. An already slower regime II further reducing its velocity in crystallized samples may be an indication that ions in this regime do not only occupy binding sites at the already oxygen rich interface but that they could also penetrate into the layer. In this context, the crystalline structure of the (Co, Fe)B grains could hinder the diffusion of ions inside the layer with respect to the amorphous case, reducing significantly the speed and efficiency of the incorporation of oxygen species. However, a detailed study of the effect of annealing on the crystalline structure of Ta/(Co, Fe)B/HfO_2 is needed to fully understand the changes observed in the magnetoionic behavior.

Regimes I and II do not only show two distinct speeds of the magnetoionic process but they also show different reversibility behaviors. The reversibility of the effects of a gate voltage of −2 V has been tested with positive gate voltages going up to +4 V in regimes I and II of as-grown samples. Higher voltages have not been applied due to the electrochemical limitations of the IL [32]. The effects of the application of +4 V for 10 min and up to 1 hour to a magnetic state close to PMA in regime I are shown in Fig. 4(a), where only minor changes are induced in the magnetic state. The same effect is found for other intermediate states in regime I and also for the fully perpendicular state, positive gate voltages up to +4 V and long exposures cannot induce a recovery of the initial under oxidized state. Regime II shows an entirely different behavior; a fully reversible transition between IPA and PMA can be observed. Figure 4(b) shows the Hall voltage hysteresis loops corresponding to reversibility cycles number 1 and 10, whereas Fig. 4(c) shows the remanence variation of the entire series. The 10 cycles show a switching of the remanence between nearly 0% (IPA) and 100% (PMA) under gate voltages of −2 and +4 V, respectively. It is interesting to note that in the first cycle, the PMA → IPA transition is induced by the application of −2 V for 1200 s, whereas for all subsequent cycles a shorter time of 240 s is required for this transition to occur. For the IPA → PMA transition, an exposure time of 600 s has been found to be sufficient for all cycles. This shows that the magnetoionic process most likely undergoes a first "activation" phase in which the first diffusion of ions involves an additional energy barrier. This could be related to the energy cost of a first detachment of the ions from their original anchoring points as well as to the formation of ionic conduction channels in the (Co, Fe)B layer, after which the ions can be moved reversibly by using significantly lower exposure times.

Regime I is therefore showing a relatively faster dynamics than in regime II under $G_V = -2$ V and a highly

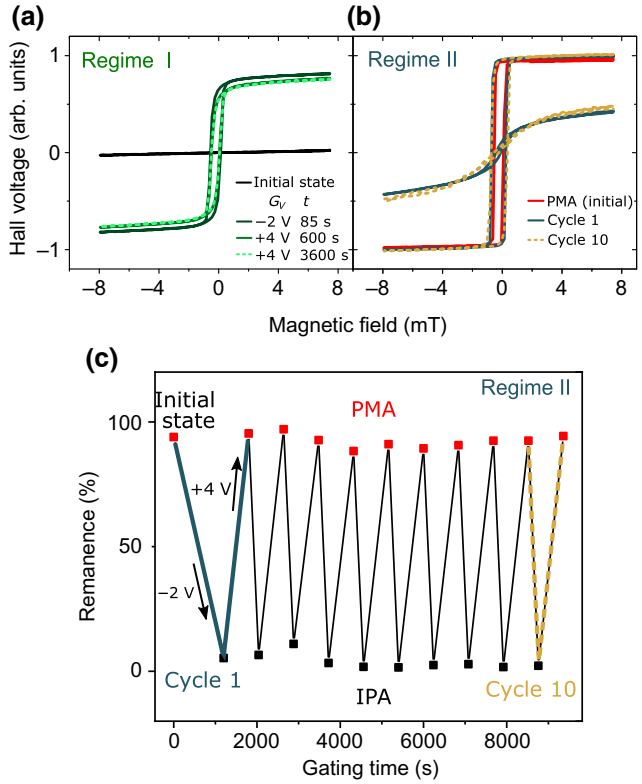

FIG. 4. (a) Suppressed reversibility of the IPA → PMA transition under $G_V = +4$ V in regime I. (b) Hysteresis loops for the reversible PMA → IPA cycles 1 (solid line) and 10 (dotted line) in regime II. (c) Remanence as a function of the reversibility cycle number in regime II.

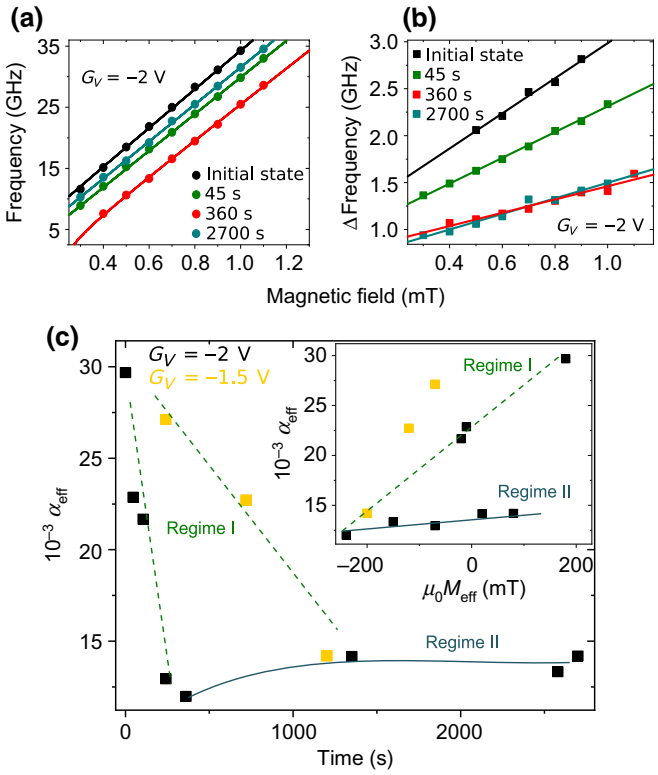

FIG. 5. (a) BLS average frequency and (b) linewidth as a function of magnetic field for an as-grown (black circles) sample, and for samples exposed to $G_V = -2$ V for 45 s (green circles), 360 s (red circles), and 2700 s (cyan circles), and the corresponding fitting lines. (c) The dependence of α_{eff} on exposure time to $G_V = -2$ V (black squares) and $G_V = -1.5$ V (yellow squares) and on $\mu_0 M_{eff}$ (inset). Lines are a guide to the eye.

suppressed reversibility at $G_V = +4$ V, whereas in regime II, a slower dynamics and full reversibility are observed. This may be linked to a high degree of stability of the final position of the ions within regime I, which would create a high-energy barrier for the inverse process, suppressing reversibility under a gate voltage of +4 V. In regime II, although the energy barrier remains asymmetric between the PMA → IPA and PMA ← IPA transitions, a gate voltage of +4 V is sufficient to revert the effects of a gate voltage of −2 V. This could be linked to a weaker anchoring of the mobile oxygen species in regime II.

III. EFFECTIVE DAMPING PARAMETER

In this section, we discuss the effect of magnetoionics on the effective damping parameter α_{eff}. A series of samples, exposed to gate voltages −2 and −1.5 V, has been investigated by Brillouin light scattering (BLS) in the Damon-Eshbach geometry after removal of the IL gate. The in-plane magnetic field dependence of the average frequency of the Stokes and anti-Stokes spin-wave frequencies was measured at a wave number $k = 8.08\ \mu m^{-1}$. Figure 5(a) shows this dependence for the as-grown sample (black circles) and for samples exposed to $G_V = -2$ V for 45 s (underoxidized, green circles), 360 s (PMA, red circles), and 2700 s (overoxidized, cyan circles). A theoretical modeling of this dependence has been performed according to [33] resulting in the fitting lines shown in Fig. 5(a). From this fitting, the values of the effective magnetization $M_{eff} = M_s - H_k$ have been obtained, where M_s and H_k are the saturation magnetization and the anisotropy field, respectively. Figure 5(b) shows the corresponding plots of the BLS frequency full linewidth (ΔF) as a function of the magnetic field applied in the plane of the sample and the corresponding fitting lines to $\Delta F = 2\alpha_{eff}(\gamma/2\pi)H + \Delta F_0$, where α_{eff} can be extracted from the slope. The dependence of α_{eff} on exposure time to a gate voltage of −2 V (black squares) and −1.5 V (yellow squares) is presented in Fig. 5(c), where the inset shows also the dependence on $\mu_0 M_{eff}$.

In regime I, the value of α_{eff} rapidly decreases from 0.029 for the as-grown sample to 0.012 for the PMA state. As shown earlier, the change from $G_V = -2$ V to $G_V = -1.5$ V critically decreases the speed of the process. In regime II, a relatively small increase in α_{eff} to 0.014 is observed, however, it does not seem to have a marked

dependence on the exposure time. This difference between regimes I and II is also expressed in the α_{eff} versus $\mu_0 M_{\text{eff}}$ dependence, where a monotonic decrease is seen in regime I, in contrast with the much-less-pronounced increase seen for regime II in a similar $\mu_0 M_{\text{eff}}$ range.

It is important to mention that the values of α_{eff} obtained from the slopes of the data points in Fig. 5(b) contain not only the intrinsic contribution from the Gilbert damping parameter but also an extrinsic contribution. This extrinsic contribution can be associated with a variety of sources including spin pumping [34–36], due to the proximity with a heavy metal with high spin-orbit coupling, two-magnon scattering [37], or the existence of sample inhomogeneities such as a distribution of anisotropy values across the sample [38,39]. The extrinsic contribution can add a relatively small factor to the value of the Gilbert damping or, in more extreme cases, it can dominate the ΔF versus H dependence resulting in the loss of linearity [38,39].

The damping parameter in (Co, Fe)B has been shown to depend on the oxidation level at the interface. In (Co, Fe)B/Gd/MgO stacks, the thin Gd layer serving as an oxygen sink has been shown to modulate the level of oxidation of an overoxidized (Co, Fe)B. In this system, α_{eff} shows a nonmonotonic dependence on the thickness of the Gd layer where a minimum is reached for 0.6 nm [40]. However, this has been linked mostly to changes in the degree of homogeneity and quality of the interface. As mentioned, the proximity and quality of the interface with a high spin orbit coupling material has been shown to induce a spin-pumping contribution to the effective damping which shows as an inverse proportionality between α_{eff} and the thickness of the magnetic film [41,42]. This additional damping contribution has been quantified for Ta by comparing symmetric MgO/(Co, Fe)B/MgO and Ta/(Co, Fe)B/Ta stacks with asymmetric Ta/(Co, Fe)B/MgO, where the Ta contribution dominates over the MgO contribution [43]. This has also been shown in the case of Hf/(Co, Fe)B/MgO stacks, which show, for a (Co, Fe)B thickness of 1.08 nm, α_{eff} values that are higher than in MgO/(Co, Fe)B/MgO stacks by about a factor of five [44].

Taking into account these considerations, it can be concluded that in the present case the underoxidized samples could have a significantly larger contact surface with Hf in HfO_2 than in the optimally oxidized case. A progression in regime I toward PMA could therefore decrease the contact surface with Hf and significantly reduce the associated spin pumping contribution to α_{eff}. Interestingly, the changes in α_{eff} are minor in regime II, which supports the idea mentioned earlier that in this regime oxygen species may migrate mostly into the layer rather than binding at the already optimally oxidized interface reached after regime I. This is considered as the main contribution to the observed variations in α_{eff}, however, a reordering of the interface structure throughout regime I is also a likely scenario. A sharper interface may be reached at the end of regime I, also leading to the highest PMA state, which could also play a role in the observed reduction of α_{eff}.

IV. DISCUSSION

The proposed magnetoionic mechanisms involved in regimes I and II are depicted in Fig. 6. For $G_V < 0$, mobile oxygen species inside HfO_2, represented as green dots, migrate toward the (Co, Fe)B layer and after G_V is switched off [Fig. 6(b)], they remain bound to the (Co, Fe)B, achieving an optimum surface coverage and completing the IPA $\rightarrow$ PMA transition at the end of regime I. If $G_V < 0$ continues to be applied, the magnetoionic mechanism will move into regime II. After the voltage is switched off [Fig. 6(c)], the incorporated oxygen species will contribute to the PMA $\rightarrow$ IPA transition. As the starting point of regime II is an optimally oxidized (Co, Fe)B surface, oxygen species incorporated in regime II will be less likely to bind at the same binding sites available in regime I and can potentially penetrate further into the layer (light green dots).

Under high enough positive gate voltages, mobile oxygen species are expected to migrate back to the top electrode [Fig. 6(d)]. However, for the same applied $G_V > 0$, reversibility is highly suppressed for oxygen species incorporated in regime I [Figs. 6(b) and 6(e)], whereas full reversibility is achieved in regime II [Figs. 6(c) and 6(f)]. This discrepancy in the degree of reversibility of regimes I and II is attributed to the differences in the binding sites, and the associated anchoring strength, of the oxygen species incorporated in each regime. The difference in chemical environment for these two types of binding sites is proposed as the origin of magnetoionic regimes I and II.

A preferential occupation of a limited number of binding sites at the (Co,Fe)B/HfO_2 interface in regime I could also explain the observed larger impact of ionic migration on the value of α_{eff} with respect to regime II. As mentioned, the effects observed may be due to a decoupling of the (Co, Fe)B surface from the Hf atoms in HfO_2, mostly linked to ion incorporation at the surface of an underoxidized (Co, Fe)B rather than to ionic migration into the layer in regime II. This is valid in a scenario where ionic migration into the layer is limited to the vicinity of the (Co,Fe)B/HfO_2 interface and does not extend up to the Ta/(Co, Fe)B interface as seen in other systems where higher gate voltages are applied [16]. It could be anticipated that ionic migration up to the Ta/(Co, Fe)B interface could induce a significant decoupling from the Ta layer, an effect observed in Pt/Co reflected as a reduction of the DMI [16], resulting in a further reduction of α_{eff}. Another important indication supporting the proposed mechanism is found in the measurements taken on crystallized samples. In this case, the time evolution of magnetic anisotropy under a negative gate voltage is strikingly reduced in

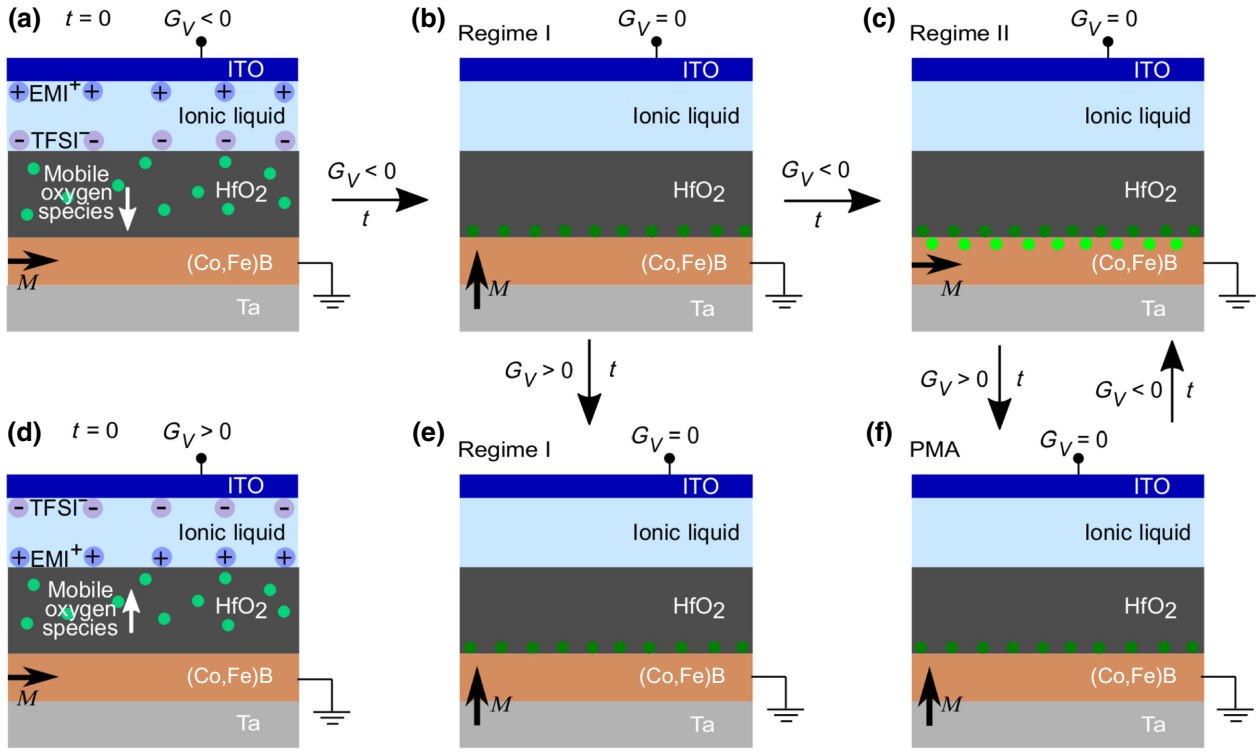

FIG. 6. Proposed magnetoionic mechanisms for regimes I and II. (a) For $G_V < 0$, oxygen species migrate toward the (Co, Fe)B layer achieving an optimum surface coverage and (b) PMA at the end of regime I. If $G_V < 0$ continues to be applied, oxygen species will continue to be incorporated into the (Co, Fe)B layer in regime II (c) resulting in IPA. Under $G_V > 0$ mobile oxygen species can migrate back to the top electrode (d). For the same applied G_V, there is no reversibility in regime I [(b) and (e)], whereas full reversibility is achieved in regime II [(c) and (f)].

regime II compared with regime I. This could be due to an increased difficulty of ionic diffusion into a crystallized (Co, Fe)B layer in regime II, compared with ionic incorporation at the surface in regime I.

Surface and bulk components to the magnetoionic effect have already been introduced in the literature, in particular, in Pd/Co/GdO_x and Pt/Co/HfO_2 films, where ion migration deep down into the magnetic layer and beyond can cause partial or total irreversibility [16,18]. As mentioned, in the present case the bulk component is thought to be limited only to the vicinity of the (Co,Fe)B/HfO_2 interface. The observed suppressed reversibility seen in regime I happens at low oxygen content, ruling out the anchoring of the oxygen species deep into the layer as a potential source of irreversibility. This is also well supported by the subsequent observation of regime II, exhibiting full reversibility, in the overoxidized state.

In this context, studies in the literature addressing the incorporation of oxygen species from the gas phase into crystalline Co and Fe systems provide an interesting perspective. In Co, the profile of the oxygen intake as a function of oxygen pressure has a distinct change in slope that is related to a two stage oxidation process. The first step involves the formation of CoO up to a defined surface coverage threshold, after which a higher oxygen and high-temperature exposure leads to the formation of Co_3O_4 [45]. In Fe crystals, a similar behavior has been observed at room temperature. The oxygen sticking coefficient as a function of surface coverage is seen to decrease drastically up to a coverage of 0.5, where an inflection point occurs followed by a less-pronounced decrease. The initial phase of rapid decrease has been linked to the filling of preferential empty binding sites, whereas additional oxygen incorporation leads to the inflection point identified as the onset of oxide growth. The oxygen incorporation is proposed to entail a progression from initially adsorbed oxygen species to the nucleation and expansion of a two-dimensional layer of FeO at the sticking coefficient inflection point, where it remains fairly constant until the completion of the FeO layer formation. Further oxygen incorporation happens in the presence of FeO, which is responsible for the observation of a reduction in the sticking coefficient after the inflection point. This last process ultimately leads to the formation of Fe_2O_3/Fe_3O_4 together with the appearance of a three-dimensional oxide structure [46,47]. In amorphous systems, the distinction between the well-defined oxide phases present in crystalline systems could be less evident, however, a distinction between

purely surface incorporation and a subsequent oxygen intake more extended into the magnetic layer could be evidenced. The films used in this study are Fe rich, with a composition of $Co_{20}Fe_{60}B_{20}$, where variations of the Fe content at the interface with an oxide have been shown to drive large PMA variations [48]. It is therefore worth considering a scenario where the formation of different Fe oxide types is at the origin of regimes I and II. Regime I is likely to reflect the initial oxygen adsorption and formation of FeO, which involves a change in valence from Fe^0 to Fe^{2+}. A significantly high-energy barrier is therefore introduced for the inverse process which would largely suppress reversibility under a low-energy stimulus. On the other hand, the full completion of a two-dimensional FeO layer could well lead to an optimum and homogeneous oxidation at the interface, allowing for the highest PMA values observable in this system. As mentioned, further oxygen incorporation in the presence of FeO becomes less favorable, which is in line with the observed slower dynamics seen in regime II. The Fe_2O_3/Fe_3O_4 oxide phase involves a mixture of Fe^{2+} and Fe^{3+} states, therefore it can be proposed that the path toward a $Fe^{2+} \rightarrow Fe^{3+}$ transition involves the progressive addition of oxygen species to the chemical environment of the Fe^{2+} centres. This phase is thought to describe regime II, where a relatively low-energy barrier is involved in the inverse process due to the conservation of the Fe^{2+} valence state. An ultimate change to Fe^{3+} would also be expected to introduce a large energy barrier for the inverse process and hinder reversibility, as seen in regime I. This is well in line with the observed behavior under $G_V = -3$ V (120 s exposure time), where the system enters an irreversible IPA overoxidized state.

V. CONCLUSION

In conclusion, we show the existence of two distinct nonvolatile magnetoionic regimes in $Ta/(Co,Fe)B/HfO_2$ stacks where oxygen species migrate under negative/positive gate voltages toward/away from the (Co, Fe)B layer. This voltage-driven ionic motion induces first an IPA $\rightarrow$ PMA transition in regime I, corresponding to a transition from an underoxidized to an optimally oxidized state. In regime II, a PMA $\rightarrow$ IPA transition occurs and it is correlated to a transition from an optimally oxidized to an overoxidized state. Regime I shows a much faster dynamics and highly suppressed reversibility for positive gate voltages with respect to regime II. In addition, it also shows a marked decrease of the effective damping parameter from 0.029 to 0.012 compared with the relatively small increase to 0.014 observed in regime II. The existence of regimes I and II is proposed to be the result of a difference in the binding strength of the migrated oxygen species, that can be correlated with different binding sites on the surface and inside the (Co, Fe)B layer, respectively.

The results presented here reveal the complexity of magnetoionics and the importance of a deep understanding of the ionic mechanisms involved in order to design robust and reliable devices for spintronics applications. This system could be easily transferred to a solid-state device where the two regimes could be probed at higher gate voltages in order to reevaluate reversibility and explore fast operation times. This will allow us to choose an IPA-to-PMA transition, either in regime I or II, that best fits the requirements for practical applications and to design strategies to favor operation in one of the two magnetoionic regimes.

ACKNOWLEDGMENTS

We gratefully acknowledge financial support from the European Union H2020 Program (MSCA ITN Grant Number 860060), from the French National Research Agency (project ELECSPIN), and the program PHC Sakura. This work was in part supported by JSPS KAKENHI Grant Number 20H05304.

[1] M. Weisheit, S. Fahler, A. Marty, Y. Souche, C. Poinsignon, and D. Givord, Electric field-induced modification of magnetism in thin-film ferromagnets, Science **315**, 349 (2007).

[2] G. H. O. Daalderop, P. J. Kelly, and M. F. H. Schuurmans, Magnetocrystalline anisotropy and orbital moments in transition-metal compounds, Phys. Rev. B **44**, 12054 (1991).

[3] K. Nakamura, R. Shimabukuro, Y. Fujiwara, T. Akiyama, T. Ito, and A. J. Freeman, Giant Modification of the Magnetocrystalline Anisotropy in Transition-Metal Monolayers by an External Electric Field, Phys. Rev. Lett. **102**, 187201 (2009).

[4] C.-G. Duan, J. P. Velev, R. F. Sabirianov, Z. Zhu, J. Chu, S. S. Jaswal, and E. Y. Tsymbal, Surface Magnetoelectric Effect in Ferromagnetic Metal Films, Phys. Rev. Lett. **101**, 137201 (2008).

[5] A. Bernand-Mantel, L. Herrera-Diez, L. Ranno, S. Pizzini, J. Vogel, D. Givord, S. Auffret, O. Boulle, I. M. Miron, and G. Gaudin, Electric-field control of domain wall nucleation and pinning in a metallic ferromagnet, Appl. Phys. Lett. **102**, 122406 (2013).

[6] Y. T. Liu, S. Ono, G. Agnus, J.-P. Adam, S. Jaiswal, J. Langer, B. Ocker, D. Ravelosona, and L. Herrera Diez, Electric field controlled domain wall dynamics and magnetic easy axis switching in liquid gated CoFeB/MgO films, J. Appl. Phys. **122**, 133907 (2017).

[7] W.-G. Wang, M. Li, S. Hageman, and C. L. Chien, Electric-field-assisted switching in magnetic tunnel junctions, Nat. Mater. **11**, 64 (2012).

[8] P.-J. Hsu, A. Kubetzka, A. Finco, N. Romming, K. von Bergmann, and R. Wiesendanger, Electric-field-driven switching of individual magnetic skyrmions, Nat. Nanotechnol. **12**, 123 (2017).

[9] M. Schott, A. Bernand-Mantel, L. Ranno, S. Pizzini, J. Vogel, H. Béa, C. Baraduc, S. Auffret, G. Gaudin,

and D. Givord, The skyrmion switch: Turning magnetic skyrmion bubbles on and off with an electric field, Nano Lett. **17**, 3006 (2017).

[10] T. Srivastava, M. Schott, R. Juge, V. Křižáková, M. Belmeguenai, Y. Roussigné, A. Bernand-Mantel, L. Ranno, S. Pizzini, S.-M. Chérif, A. Stashkevich, S. Auffret, O. Boulle, G. Gaudin, M. Chshiev, C. Baraduc, and H. Béa, Large-voltage tuning of Dzyaloshinskii–Moriya interactions: A route toward dynamic control of skyrmion chirality, Nano Lett. **18**, 4871 (2018).

[11] T. Koyama, Y. Nakatani, J. Ieda, and D. Chiba, Electric field control of magnetic domain wall motion via modulation of the Dzyaloshinskii-Moriya interaction, Science Advances **4**, eaav0265 (2018).

[12] S. Zhang, Spin-Dependent Surface Screening in Ferromagnets and Magnetic Tunnel Junctions, Phys. Rev. Lett. **83**, 640 (1999).

[13] U. Bauer, S. Emori, and G. S. D. Beach, Voltage-controlled domain wall traps in ferromagnetic nanowires, Nat. Nanotechnol. **8**, 411 (2013).

[14] U. Bauer, L. Yao, A. J. Tan, P. Agrawal, S. Emori, H. L. Tuller, S. van Dijken, and G. S. D. Beach, Magneto-ionic control of interfacial magnetism, Nat. Mater. **14**, 174 (2015).

[15] R. Mishra, F. Mahfouzi, D. Kumar, K. Cai, M. Chen, X. Qiu, N. Kioussis, and H. Yang, Electric-field control of spin accumulation direction for spin-orbit torques, Nat. Commun. **10**, 248 (2019).

[16] L. Herrera Diez, *et al.*, Nonvolatile Ionic Modification of the Dzyaloshinskii-Moriya Interaction, Phys. Rev. Appl. **12**, 034005 (2019).

[17] G. Chen, A. Mascaraque, H. Jia, B. Zimmermann, M. Robertson, R. L. Conte, M. Hoffmann, M. A. G. Barrio, H. Ding, R. Wiesendanger, E. G. Michel, S. Blügel, A. K. Schmid, and K. Liu, Large Dzyaloshinskii-Moriya interaction induced by chemisorbed oxygen on a ferromagnet surface, Sci. Adv. **6**, eaba4924 (2020).

[18] D. A. Gilbert, A. J. Grutter, E. Arenholz, K. Liu, B. J. Kirby, J. A. Borchers, and B. B. Maranville, Structural and magnetic depth profiles of magneto-ionic heterostructures beyond the interface limit, Nat. Commun. **7**, 12264 (2016).

[19] A. J. Tan, M. Huang, C. O. Avci, F. Büttner, M. Mann, W. Hu, C. Mazzoli, S. Wilkins, H. L. Tuller, and G. S. D. Beach, Magneto-ionic control of magnetism using a solid-state proton pump, Nat. Mater. **18**, 35 (2019).

[20] K.-Y. Lee, S. Jo, A. J. Tan, M. Huang, D. Choi, J. H. Park, H.-I. Ji, J.-W. Son, J. Chang, G. S. D. Beach, and S. Woo, Fast magneto-ionic switching of interface anisotropy using yttria-stabilized zirconia gate oxide, Nano Lett. **20**, 3435 (2020).

[21] A. Fassatoui, J. P. Garcia, L. Ranno, J. Vogel, A. Bernand-Mantel, H. Bea, S. Pizzini, and S. Pizzini, Reversible and Irreversible Voltage Manipulations of Interfacial Magnetic Anisotropy in Pt/Co/Oxide Multilayers, Phys. Rev. Appl. **14**, 064041 (2020).

[22] C. Leighton, Electrolyte-based ionic control of functional oxides, Nat. Mater. **18**, 13 (2019).

[23] J. Jeong, N. Aetukuri, T. Graf, T. D. Schladt, M. G. Samant, and S. S. P. Parkin, Electrolyte-based ionic control of functional oxides, Science **339**, 1402 (2013).

[24] J. Shi, S. D. Ha, Y. Zhou, F. Schoofs, and S. Ramanathan, A correlated nickelate synaptic transistor, Nat. Commun. **4**, 2676 (2013).

[25] S. Ono, S. Seki, R. Hirahara, Y. Tominari, and J. Takeya, High-mobility, low-power, and fast-switching organic field-effect transistors with ionic liquids, Appl. Phys. Lett. **92**, 103313 (2008).

[26] A. Manchon, C. Ducruet, L. Lombard, S. Auffret, B. Rodmacq, B. Dieny, S. Pizzini, J. Vogel, V. Uhlí, M. Hochstrasser, and G. Panaccione, Analysis of oxygen induced anisotropy crossover in Pt/Co/MO_x trilayers, J. Appl. Phys. **104**, 043914 (2008).

[27] T. Nagata, M. Haemori, Y. Yamashita, H. Yoshikawa, Y. Iwashita, K. Kobayashi, and T. Chikyow, Oxygen migration at Pt/HfO_2/Pt interface under bias operation, Appl. Phys. Lett. **97**, 082902 (2010).

[28] S. Yuasa, Y. Suzuki, T. Katayama, and K. Ando, Characterization of growth and crystallization processes in CoFeB/MgO/CoFeB magnetic tunnel junction structure by reflective high-energy electron diffraction, Appl. Phys. Lett. **87**, 242503 (2005).

[29] W. G. Wang, J. Jordan-sweet, G. X. Miao, C. Ni, A. K. Rumaiz, L. R. Shah, X. Fan, P. Parsons, R. Stearrett, E. R. Nowak, J. S. Moodera, and J. Q. Xiao, In-situ characterization of rapid crystallization of amorphous CoFeB electrodes in CoFeB/MgO/CoFeB junctions during thermal annealing, Appl. Phys. Lett. **95**, 242501 (2009).

[30] J. Sinha, M. Gruber, M. Kodzuka, T. Ohkubo, S. Mitani, K. Hono, and M. Hayashi, Influence of boron diffusion on the perpendicular magnetic anisotropy in Ta/CoFeB/MgO ultrathin films, J. Appl. Phys. **117**, 043913 (2015).

[31] B. F. Vermeulen, J. Wu, J. Swerts, S. Couet, I. P. Radu, G. Groeseneken, C. Detavernier, J. K. Jochum, M. V. Bael, K. Temst, A. Shukla, S. Miwa, Y. Suwuki, and K. Martens, Perpendicular magnetic anisotropy of CoFeB/Ta bilayers on ALD HfO_2, AIP. Adv. **7**, 055933 (2017).

[32] J. Seidemann, Ph.D. thesis, Université Grenoble Alpes, 2017.

[33] M. Belmeguenai, J.-P. Adam, Y. Roussigné, S. Eimer, T. Devolder, J.-V. Kim, S. M. Cherif, A. Stashkevich, and A. Thiaville, Interfacial Dzyaloshinskii-Moriya interaction in perpendicularly magnetized Pt/Co/AlO_x ultrathin films measured by Brillouin light spectroscopy, Phys. Rev. B **91**, 180405 (2015).

[34] H. Nakayama, K. Ando, K. Harii, T. Yoshino, R. Takahashi, Y. Kajiwara, K. Uchida, Y. Fujikawa, and E. Saitoh, Geometry dependence on inverse spin Hall effect induced by spin pumping in $Ni_{81}Fe_{19}$/Pt films, Phys. Rev. B **85**, 144408 (2012).

[35] M. Belmeguenai, M. S. Gabor, F. Zighem, N. Challab, T. Petrisor, R. B. Mos, and C. Tiusan, Ferromagnetic-resonance-induced spin pumping in $Co_{20}Fe_{60}B_{20}$/Pt systems: Damping investigation, J. Phys. D: Appl. Phys. **51**, 045002 (2018).

[36] M. Belmeguenai, D. Apalkov, Y. Roussigné, M. Chérif, A. Stashkevich, G. Feng, and X. Tang, Exchange stiffness and damping constants in diluted $Co_xFe_yB_{1-x-y}$ thin films, J. Phys. D: Appl. Phys. **50**, 415003 (2017).

[37] B. K. Kuanr, R. E. Camley, and Z. Celinski, Extrinsic contribution to Gilbert damping in sputtered NiFe films by

ferromagnetic resonance, J. Magn. Magn. Mater. **286**, 276 (2005).

[38] A. Capua, S.-h. Yang, T. Phung, and S. S. P. Parkin, Determination of intrinsic damping of perpendicularly magnetized ultrathin films from time-resolved precessional magnetization measurements, Phys. Rev. B **92**, 224402 (2015).

[39] L. H. Diez, M. Voto, A. Casiraghi, M. Belmeguenai, Y. Roussigné, G. Durin, A. Lamperti, R. Mantovan, V. Sluka, V. Jeudy, Y. T. Liu, A. Stashkevich, S. M. Chérif, J. Langer, B. Ocker, L. Lopez-Diaz, and D. Ravelosona, Enhancement of the Dzyaloshinskii-Moriya interaction and domain wall velocity through interface intermixing in Ta/CoFeB/MgO, Phys. Rev. B **99**, 054431 (2019).

[40] G. Yang, J.-Y. Zhang, S.-L. Jiang, B.-W. Dong, S.-G. Wang, J.-L. Liu, Y.-C. Zhao, C. Wang, Y. Sun, and G.-H. Yu, Effect of oxygen migration on magnetic anisotropy and damping constant in perpendicular Ta/CoFeB/Gd/MgO/Ta multilayers, Appl. Surf. Sci. **396**, 705 (2017).

[41] S. Ikeda, K. Miura, H. Yamamoto, K. Mizunuma, H. D. Gan, M. Endo, S. Kanai, J. Hayakawa, F. Matsukura, and H. Ohno, A perpendicular-anisotropy CoFeB–MgO magnetic tunnel junction, Nat. Mater. **9**, 721 (2010).

[42] I. Benguettat-El Mokhtari, Y. Roussigné, S. M. Chérif, A. Stashkevich, S. Auffret, C. Baraduc, M. Gabor, H. Béa, and M. Belmeguenai, Interface phenomena in ferromagnet/TaO_x-based systems: Damping, perpendicular magnetic anisotropy, and Dzyaloshinskii-Moriya interaction, Phys. Rev. Mater. **4**, 124408 (2020).

[43] S. Iihama, S. Mizukami, H. Naganuma, M. Oogane, Y. Ando, and T. Miyazaki, Gilbert damping constants of Ta/CoFeB/MgO(Ta) thin films measured by optical detection of precessional magnetization dynamics, Phys. Rev. B **89**, 174416 (2014).

[44] J. Lourembam, A. Ghosh, M. Zeng, S. K. Wong, Q. J. Yap, and S. Ter Lim, Thickness-Dependent Perpendicular Magnetic Anisotropy and Gilbert Damping in $Hf/Co_{20}Fe_{60}B_{20}/MgO$ Heterostructures, Phys. Rev. Appl. **10**, 044057 (2018).

[45] M. E. Bridge and R. M. Lambert, Oxygen chemisorption, surface oxidation, and the oxidation of carbon monoxide on cobalt (0001), Surf. Sci. **82**, 413 (1979).

[46] C. Brundle, Oxygen adsorption and thin oxide formation at iron surfaces: An XPS/UPS study, Surf. Sci. **66**, 581 (1977).

[47] G. W. Simmons and D. J. Dwyer, A LEED-AES study of the initial stages of oxidation of Fe(001), Surf. Sci. **48**, 373 (1975).

[48] L. Herrera Diez, F. García-Sánchez, J.-P. Adam, T. Devolder, S. Eimer, M. S. El Hadri, A. Lamperti, R. Mantovan, B. Ocker, and D. Ravelosona, Controlling magnetic domain wall motion in the creep regime in He^+-irradiated CoFeB/MgO films with perpendicular anisotropy, Appl. Phys. Lett. **107**, 032401 (2015).